6 Techniques for PBI Membrane Characterization

Dirk Henkensmeier and David Aili

6.1 Introduction

The purpose of this chapter is to introduce common methods used for characterization of membranes, especially of polybenzimidazole (PBI) derivative based membranes. Initially we planned also to provide detailed standard procedures for each method, but quickly decided that while some standards need to be maintained, each lab will need adjustments, e.g., where parameters vary based on the used equipment or material. We hope that this text will be a good guidance for newcomers, will raise awareness of the scopes and limitations of the discussed methods, and will help researchers to develop or improve their own standard procedures.

To get reproducible values and data for statistical calculations, multiple samples should be analyzed wherever possible. The given drying times should be considered as a rule of thumb, which will give reasonably accurate values. The best guideline is to dry until constant weight is reached, because drying processes depend on several factors, including the membrane thickness.

6.2 Molecular Weight of PBI

6.2.1 Definitions

A distinguishing characteristic of polymeric materials is their molecular weight (g mol^{-1}). The number of repeat units in a macromolecular chain is termed the degree of polymerization (DP). For a polymer consisting of repeat units of the relative molecular mass M_{PRU}, the molecular weight is defined as $M = DP \times M_{PRU}$. Techniques more commonly used for the determination of molecular weights of polymers include osmometry, light scattering, and ultracentrifugation, although titration (end-group analysis), cryoscopy, and ebulliometry are also used in some applications. As the molecular weight values obtained vary to a large extent with the measuring methods, there are different definitions of the molecular weight. In general, an average molecular weight is expressed by (6.1), where N_i is the number of macromolecules having a molecular weight of M_i.

D. Henkensmeier (✉)
Fuel Cell Research Center, Korea Institute of Science and Technology, Hwarangro 14gil5, SeongbukguSeoul 136-791, South Korea
e-mail: henkensmeier@kist.re.kr

D. Aili
Proton Conductors Section, Department of Energy Conversion and Storage, Technical University of Denmark, Kemitorvet 207, Kgs. Lyngby 2800, Denmark
e-mail: larda@dtu.dk

Q. Li et al. (eds.), *High Temperature Polymer Electrolyte Membrane Fuel Cells*,
DOI 10.1007/978-3-319-17082-4_6

$$\overline{M} = \frac{\sum_{i=1}^{N} N_i M_i^{\alpha}}{\sum_{i=1}^{N} N_i M_i^{\alpha-1}} \tag{6.1}$$

For $\alpha = 1$ the number average molecular weight $\overline{M}_n$ is obtained from (6.2).

$$\overline{M}_n = \frac{\sum_{i=1}^{N} N_i M_i}{\sum_{i=1}^{N} N_i} \tag{6.2}$$

Methods that depend on end-group analysis or colligative properties (freezing-point depression, boiling-point elevation, osmotic pressure) can be employed to determine $\overline{M}_n$.

For $\alpha = 1$, the weight average molecular weight $\overline{M}_w$ is thus obtained from (6.3), and usually determined by light scattering or ultracentrifugation.

$$\overline{M}_w = \frac{\sum_{i=1}^{N} N_i M_i^2}{\sum_{i=1}^{N} N_i M_i} \tag{6.3}$$

The ratio between the weight average molecular weight and the number average molecular weight is called polydispersity index (PDI), as given by (6.4). For synthetic polymers $\overline{M}_w > \overline{M}_n$, which implies that PDI > 1.

$$\text{PDI} = \frac{\overline{M}_w}{\overline{M}_n} \tag{6.4}$$

6.2.2 Viscosity

The most convenient method for routinely determining molecular weights is to measure the viscosity of a polymer containing solution. This is not an absolute method and it should thus be used in combination with one of the techniques of measuring the absolute molecular weight.

The molecular weight of PBI strongly influences the membrane properties and the lifetime of the membrane electrode assembly (MEA), as shown by Yang et al. [1]. Due to the poor solubility of PBI in common solvents such as tetrahydrofurane (THF) or acetonitrile, the most common method to evaluate the molecular weight of PBI is to measure the viscosity dissolved in 96 % sulfuric acid. Care needs to be taken not to heat sulfuric acid-based PBI solutions and not to store them for a long time, to avoid possible side reactions like sulfonation or cross-linking. Also, viscosity depends on temperature, and a strict control of the temperature is necessary. Impurities like dust should be removed by filtration.

To obtain the molecular weight from viscosity measurements, PBI is dissolved in concentrated sulfuric acid to give a solution with a solid content in the range of typically 2–5 g L^{-1}. The viscosity of polymer solutions is usually measured with an Ubbelohde viscometer. To prepare for the measurement, the solution is first sucked through a capillary into a reservoir. During the measurement, the solution is allowed to flow back through the capillary and the flow time of the upper solution level between two marks on the capillary is noted.

The relative viscosity (η_{rel}) and the specific viscosity (η_{sp}) should be determined at different polymer concentrations according to (6.5) and (6.6), respectively, where t and t_0 are the flow time of the polymer solution and pure solvent, respectively.

$$\eta_{\text{rel}} = t/t_0 \tag{6.5}$$

$$\eta_{\text{sp}} = (t - t_0)/t_0 \tag{6.6}$$

The specific viscosities are measured for a series of polymer solutions of varied polymer concentrations, which can easily be done by diluting the initial polymer solution. The obtained specific viscosities are then divided by the respective concentration, to give the reduced viscosity (η_{red}). As can be seen from (6.7), the intrinsic viscosity (η_{IV}) of the polymer solution is

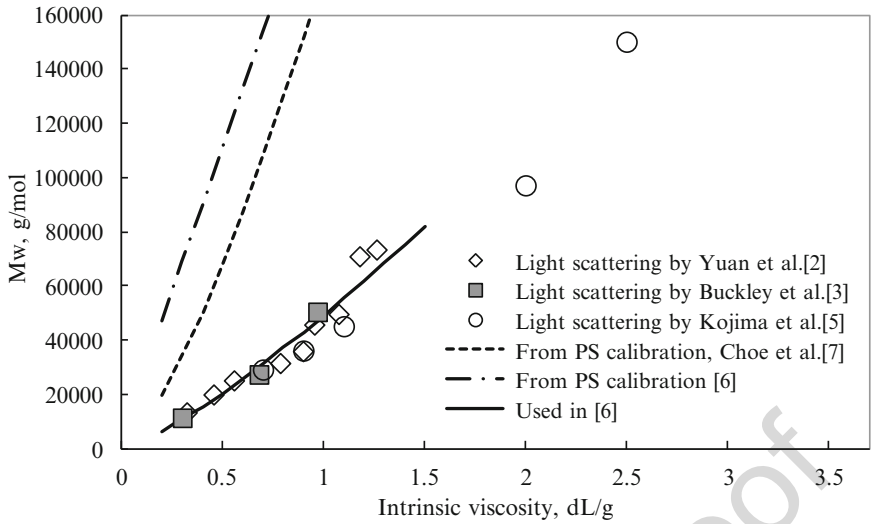

Fig. 6.1 The relation between intrinsic viscosity and polymer molecular weight. Reproduced from [6] with permission of John Wiley and Sons

obtained by plotting the reduced viscosity against the polymer concentration (c) and extrapolating to zero concentration.

$$\eta_{\text{red}}[\text{mL/g}] = \frac{\eta_{\text{sp}}}{c} = \eta_{\text{IV}} + k \cdot \eta_{\text{IV}}^2 \cdot c \qquad (6.7)$$

Alternatively the intrinsic viscosity (η_{IV}) can be estimated from a single point measurement by using (6.8), which showed more than 99 % accuracy at relatively low concentrations [2].

$$\eta_{\text{IV}}[\text{dL/g}] = \left(\eta_{\text{sp}} + 3\ln\left(1 + \eta_{\text{sp}}\right)\right)/4c \qquad (6.8)$$

The weight averaged molecular weight $\left(\overline{M}_{\text{w}}\right)$ can subsequently be obtained from the Mark–Houwink expression as shown in (6.9), where K and α are the empirical Mark–Houwink constants, depending on the molecular weight range and molecular weight distribution.

$$\eta_{\text{IV}} = K \times \overline{M}_{\text{w}}^{\alpha} \qquad (6.9)$$

Mark–Houwink constants of $K = 1.94 \times 10^{-4}$ dL g^{-1} and $\alpha = 0.791$ can be extracted from light scattering data published by Buckley et al. [3, 4]. Mark–Houwink constants of $K = 4.7 \times 10^{-4}$ dL g^{-1} and $\alpha = 0.93$ were published by Yuan et al. [2], based on PBI of a molecular weight between 13,200 and 70,800 g mol^{-1} and a PDI of less than 2, obtained by fractionation with DMF at 152 °C. Light scattering and viscosity of PBIs up to the very high molecular weight of 230,000 g mol^{-1} were measured by Kojima et al. [5]. As shown in Fig. 6.1, the three sets of the constants agree to a satisfactory extent within the low intrinsic viscosity range <1.5 dL g^{-1}.

Since the determination of the molecular weight strongly depends on the way it is measured, often only the inherent viscosity (η_{inh}) of PBI derivatives is reported. It can be obtained from the relation in (6.10).

$$\eta_{\text{inh}} = \ln(\eta_{\text{rel}})/c \qquad (6.10)$$

This can be obtained from a single point measurement, but the used concentration should be specified. The inherent viscosity is especially useful to compare the degree of polymerization of different polymer batches, either as quality control or as a means to find the optimum polymerization conditions. Typical conditions are a temperature of 30 °C, a polymer solution with a solid content of 2 g L^{-1} and a Cannon Ubbelohde viscometer with a 200 µm capillary [8].

6.2.3 Size Exclusion Chromatography

Size exclusion chromatography (SEC), which is also called gel permeation chromatography (GPC), is a method to separate macromolecules with respect to size. As the names already suggest, a polymer solution passes a column filled with a porous gel phase. The pore size in that gel phase varies from, say, 10–100 nm. When a polymer solution passes through the column the individual polymer molecules are separated according to their hydrodynamic radius. The underlying principal is that smaller molecules can enter the pores of the gel phase easier than larger polymer chains, leading to retention of smaller molecules and fast elution of the higher molecular weight macromolecules. At the end of the column, one or two detectors continuously record, e.g., the refractive index (RI) or the ultraviolet (UV) spectrum of the passing solution.

In brief, SEC is a method giving rapid access to the weight distribution (e.g., single or binodal distribution), number and weight average molar mass and thus the PDI. Measurements can be carried out using very small amounts of polymer (e.g., 30 µL injection volume at a concentration of 3 mg mL^{-1}). Figure 6.2 shows the molecular weight distribution for a PBI-based copolymer obtained from SEC measurements.

In order to correlate the elution time with the molecular weight, calibration with polymers of a known, narrow molecular weight distribution is necessary. Most researchers calibrate the column against commercial standards (e.g., polystyrene or poly(methyl methacrylate) (PMMA)), which can be prepared with a narrow molecular weight distribution by living polymerization. Special care should be taken with this calibration. A large deviation is expected because the polarity of, e.g., PS and PBI is so different, that other eluents should be used in their SEC measurements. Furthermore, the hydrodynamic radius of the investigated polymer in the chosen solvent system is always different from that of the calibration standard. Another practical issue is that the polymer solutions need to be free from impurities to prevent clogging, and filtration through 0.45 µm PTFE syringe filters may in some cases slightly influence the sample composition.

It should be remarked that the literature work on the SEC analysis has been conducted under very much varied conditions. Table 6.1 gives a few examples. In these works, the system was calibrated against polystyrene or PMMA standards, and the eluents contained lithium salts to prevent PBI agglomeration. The reader should keep this in mind when a comparison of the results is done.

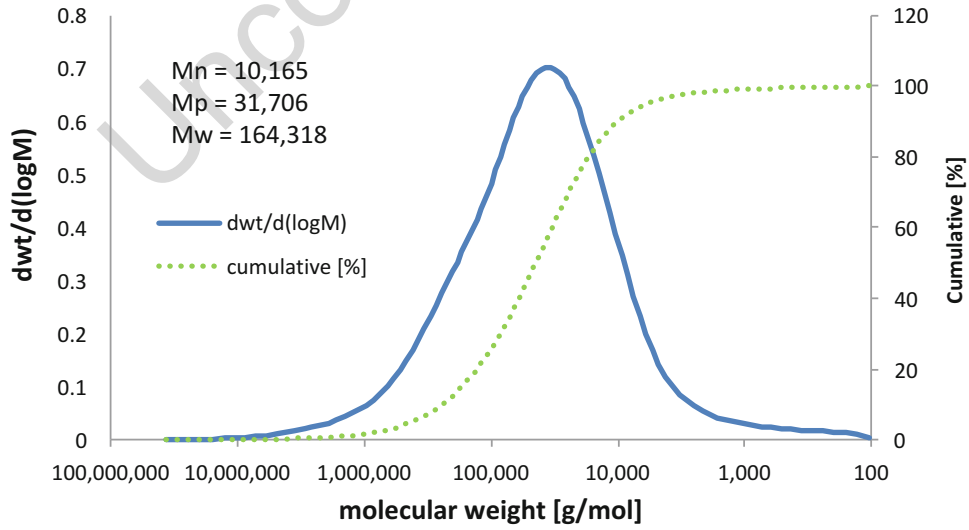

Fig. 6.2 Molecular weight distribution for a PBI-based copolymer obtained from SEC measurements [9]

t.1 **Table 6.1** Conditions for SEC analysis of PBI derivatives

t.2 Polymer	Solvents and other experimental details	Reference
t.3 *meta*-PBI	DMAc + 0.5 wt% LiCl; 40 °C; RI as detector; two columns having a pore size range from 102 to 106 Å; flow rate of 0.2 mL min^{-1}	[6]
t.4 Sulfonated PBI block-copolymer	DMSO/DMF (1/10) mixture; eluent: 0.01 mol L^{-1} LiBr DMF solution; UV as detector; column: Shodex KF-805 and Shodex SB-803HQ	[10]
t.5 *meta*-PBI and *N*-alkylated *meta*-PBI	0.5 wt% LiBr in NMP; 70 °C; UV and RI as detector; column: GRAM 100 and 1000 Å columns (PSS, Mainz, Germany); flow rate: 0.8 mL min^{-1}	[11]
t.6 *meta*-PBI and *N*-alkylated *meta*-PBI	0.5 wt% LiBr in DSMO; 70 °C; UV and RI as detector; column: 2 PSS GRAL LIN columns; flow rate: 1.0 mL min^{-1}	[11]
t.7 Sulfonated PBI derivative	0.01 mol L^{-1} LiBr in DMF; 70 °C; column: mixed 10 μm PS column with a length of 750 mm; flow rate: 1.0 mL min^{-1}	[12]
t.8 PBI copolymer	0.05 mol L^{-1} LiBr in NMP; 45 °C; RI as detector; column: 2 TSKgel Alpha-M columns (Tosoh Bioscience); flow rate: 1.0 mL min^{-1}	[9]

t.9 The reader is referred to the original work for further experimental details and complete polymer structures

6.3 Water and Phosphoric Acid Uptake

6.3.1 Water Uptake of Pristine PBI Membranes

PBI derivatives are well known to be highly hydrophilic. The water uptake from the liquid phase can be obtained by submerging a pristine membrane in distilled water. After a certain period of time, typically a few days at room temperature, the membrane is taken out of the water, quickly blotted with a tissue, and weighed immediately. Theoretically it should not matter if the wet or dry weight is obtained first. However, PBI membranes produced by solution casting may still contain some organic solvent, which cannot be removed completely by drying unless very high temperatures are applied, but which may leach out in contact with liquid water. In connection to all the weight measurements of membranes it is thus a general good practice to ensure that the membrane is free from residual organic solvents (e.g., dimethylacetamide, DMAc) and other impurities such as stabilizers (e.g., LiCl).

To determine the water uptake of a pristine membrane from the vapor phase at different humidities and room temperature, a membrane sample can be suspended above a LiCl aqueous solution in a closed vessel. The relative humidity of the atmosphere above a lithium chloride solution versus the concentration is well defined and known [13]. More than 10 days have been suggested to reach equilibrium.

The water uptake (WU) of a membrane is often reported in percent and defined on the dry polymer basis and calculated by comparing the dry weight (W_{dw}) and the wet weight (W_{ww}) of a membrane according to (6.11)

$$\mathrm{WU}\ [\%] = 100 \cdot (W_{ww} - W_{dw})/W_{dw} \quad (6.11)$$

6.3.2 Phosphoric Acid Uptake

When membranes are doped by immersion in an aqueous phosphoric acid (PA) solution the weight gain is due to both acid and water uptake. To distinguish between the contributions to the weight gain from water and acid, the membrane should be dried (e.g., at 110 °C for at least 5 h in vacuo [14]). This process is assumed to remove all the water, and the remaining PA is considered as 100 % PA. According to Majerus et al. [15], further dehydration of phosphoric acid is slowed down by interactions with the polymer chains, and the thermogravimetric analysis (TGA) curve of PA doped ABPBI shows a plateau between

90 and 110 °C. If the weight fraction of the polymer is not known, the membranes need to be de-doped to obtain the polymer content (W_{PBI}). The de-doping can be achieved by immersion of the doped membranes in a large amount of water followed by drying in vacuo at 110 °C [16]. A few hours may be needed under stirring at room temperature or with gentle heating, preferably in dilute alkaline solutions such as aqueous NaOH or NH_4OH [17]. Alternatively the phosphoric acid and water content of PA-doped membranes can be determined by titration with NaOH [16, 18]. In order to determine the acid uptake by titration, PA is first leached out by immersion of the doped membrane in (warm) water [16]. The water is then titrated with aqueous NaOH and the PA doping level can be calculated based on the volume and concentration of spent titer.

In analogy with the water uptake, the acid uptake (AU) of a membrane is often given in percent on the dry polymer basis as the ratio between the phosphoric acid content (W_{PA}) and the PBI content (W_{PBI}) of the membrane (6.12).

$$\mathrm{AU}\ [\%] = 100 \cdot W_{PA}/W_{PBI} \tag{6.12}$$

Sometimes the amount of acid is also reported as the acid content (AC) on the doped membrane basis according to (6.13).

$$\mathrm{AC}\ [\%] = 100 \cdot W_{PA}/(W_{PBI} + W_{PA}) \tag{6.13}$$

The term acid doping level (ADL) is widely used and is defined as the number of phosphoric acid molecules per polymer repeat unit and can be calculated according to (6.14), where M_{PBI} is the molar mass of the polymer repeat unit and M_{PA} is the molar mass of PA.

$$\mathrm{ADL} = (W_{PA} \times M_{PA})/(W_{PBI} \times M_{PBI}) \tag{6.14}$$

The term ADL allows for a direct comparison of the phosphoric acid content of polymers of the same type. However, since the molar mass of the polymer repeat unit varies with its structure, it does not allow for a direct comparison of the phosphoric acid content for structurally different polymers. It should also be remembered that any incomplete extraction of the acid would lead to underestimation of the ADL.

6.3.3 Dimensional Changes

The water and phosphoric acid uptake cause dimensional changes of the membrane (swelling). The swelling is normally calculated on the dry undoped membrane volume basis according to (6.15), where $V_{undoped}$ and V_{doped} are the volume of the undoped and doped membrane, respectively.

$$\mathrm{Swelling}\ [\%] = 100 \cdot \left(V_{doped} - V_{undoped}\right)/V_{undoped} \tag{6.15}$$

The volume of the undoped (usually of the fully dried membrane) and doped membrane can readily be calculated from the dimensional changes of the membrane. The dimensional changes of a membrane can be divided into the length, width, or thickness (for linear swelling), the area (for two dimensional swelling) or volume (for three dimensional swelling). At the first glance, the linear expansion in x, y and z direction should be the same, however, this is not always the case. One reason for anisotropic swelling is that extruded membranes have a machine and a transverse direction, and the polymer chain orientation is preferably in the machine direction. A similar effect may also be observed if an initially isotropic membrane is stretched during processing, e.g., in roll-to-roll processes like drying or cutting. Care must also be taken that swollen, soft membranes are not indented during the thickness measurement. This risk can be reduced by equipping the thickness gauge with an appropriately broad tip or by sandwiching the membrane between sheets of a support material.

6.4 Conductivity

6.4.1 Definitions and Equations

Proton conductivity, the ability of a material to pass an electric current by the movement of protons, is one of the key characteristics of electrolytes. The opposition of the material to the passage of current is called resistance, which is measured from the voltage loss (V)

across the material upon the current passage. For an object with a uniform cross-section, for example a strip of a film, its resistance (R) is proportional to its resistivity (ρ) and length (L) and inversely proportional to its cross-sectional area (A) by Pouillet's law (6.16).

$$R\,[\Omega] = \rho\frac{L}{A} = \frac{1}{\sigma}\cdot\frac{L}{A} \tag{6.16}$$

Here σ is the conductivity or the reciprocal of the resistivity, having a unit of ohm^{-1} cm^{-1} or more commonly S cm^{-1}. In electrochemical devices, the area-specific resistance (ASR, ohm cm^2) of a flat sheet membrane electrolyte is of engineering importance and can be expressed as the product of the resistance and the surface area, or as the ratio between the thickness and the conductivity. The ASR is directly proportional to the voltage loss (V) of the electrolyte at the current density i (A cm^{-2}), because $V = \text{ASR} \times i$. The expression of the thickness to conductivity ratio indicates that high conductivity (σ) and small electrolyte thickness (L) lead to a low cell resistance.

6.4.2 Conductivity Cells

The accuracy of conductivity measurements can be influenced by several factors including polarization, sample dimensions, contact point resistance, cable/wire resistance or capacitance, and most importantly temperature and humidity (particularly for proton conductivity).

For the conductivity measurement, applying a current through the electronically conducting electrodes to the ionically conducting membrane causes a polarization at the interface due to the electron transfer reaction and concentration changes of active species. Any polarization resistance arising at the electrode surface leads to erroneous results as it is a parasitic component to the resistance. One way to eliminate the polarization effect is to introduce two reference electrodes through which the voltage signals are measured. As there is no current flowing through these reference electrodes, no polarization is developed or included in the measurement. The electrode and membrane geometries for the four-probe method are shown in Fig. 6.3. In analogy to

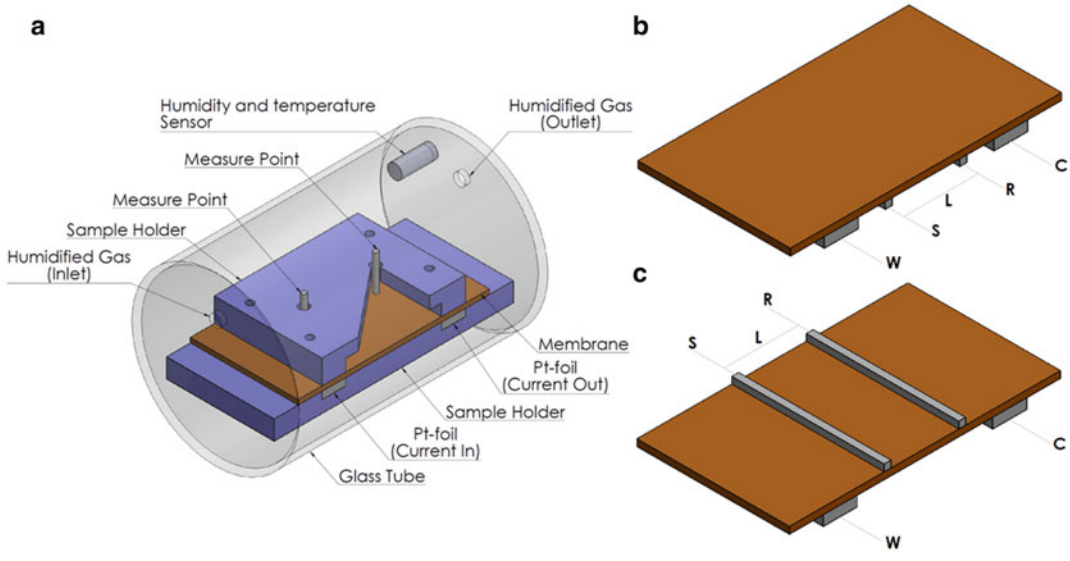

Fig. 6.3 Construction of a four-probe conductivity cell (**a**) and electrode assembling for in-plane (**b**) and mixed in-plane and through plane (**c**) conductivity measurements

a potentiostat, the two current supplying electrodes are marked as working (W) and counter (C) while the other two for voltage measurements are marked as reference (R) and sense (S) electrodes. When all four electrodes are located on the same side of the membranes (Fig. 6.3b) the resistance is recorded in the plane of the membrane. When the current supplying electrodes (W and C) and voltage measuring (R and S) electrodes are located on the opposite sides of the membranes (Fig. 6.3c), the resistance is measured in-plane, but reduces the risk of surface effects. For through-plane conductivity measurements, W and R are placed on one side of the membrane and C and S on the other.

A four-probe conductivity cell is schematically represented in Fig. 6.3a. Here, the membrane is fixed between two sample holders. The upper one is made of glass and shows two holes for the potential sensing electrodes (R and S). The distance between the two platinum electrodes is 1 cm. The lower sample holder contains two platinum bands as current supplying electrodes (C and W). The cell is assembled into a glass tube, which has two endplates through which electrical connections and humidified air inlet and outlet are fixed with gas tight seals. The whole cell is kept in an oven for temperature control. Some groups also use platinum tips in a vertical arrangement instead of horizontal wires as potential electrodes [19].

In such measurements, it is assumed that the current is homogeneously distributed throughout the entire membrane cross-section. Any membrane inhomogeneity is problematic. For PA-doped membranes, a thin liquid film may be formed at high humidities at temperatures around or below 100 °C at atmospheric pressure. In this case the measured conductivity is mainly from the highly conductive surface layer. Mixed in-plane/through-plane assembling minimizes this risk to some extent.

Alternatively the through-plane conductivity is often measured with two electrode cells. The cell can be similar to a fuel cell where the membrane is sandwiched between two electrodes. The electrodes typically consist of platinum disks or gas diffusion electrode diffusion electrodes covering the entire membrane area. The latter allows to measure conductivity under varied atmospheric humidities, but with longer equilibration times than for in-plane cells. For these cells, it is critical to minimize the polarization effect, which can be sufficiently achieved by using a high frequency alternating current, as to be discussed below. A hydrogen flow, as a humidification carrier gas, is recommended on both electrode chambers, because its high electrochemical reversibility further reduces the polarization. Figure 6.4 schematically shows the effect of the uncovered part of the membrane at the edge of the active electrode area. Any mismatching of the electrodes will have a similar effect, i.e., leading to current along the membrane thickness direction.

The contact resistance in the cell is a major source of error for through-plane measurements, and should be registered for each type of material by a series of measurements with membranes of different thickness. A plot of the measured

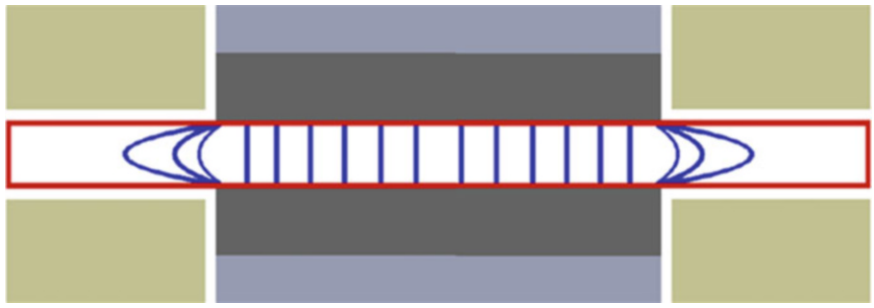

Fig. 6.4 Membrane electrode assembly and current distribution at the membrane edge

resistance against the membrane thickness allows one to obtain the contact resistance (y-axis intercept) and the membrane resistance (slope). Assuming that the resistance between two membrane layers is negligible, also stacks of membrane samples can be used instead of samples with different thickness. Obviously care must be taken to avoid gas bubbles between the layers, which would be insulating and increasing the thickness.

In general, for conductivity measurements two types of alternating current are used, i.e., the square wave current (also called direct current interruption) or electrochemical impedance spectroscopy (EIS). For EIS, the AC frequency is often in a range from 0.1 to 1 MHz down to 1–10 Hz. A more detailed discussion on these techniques is not attempted in this chapter. In theory, the high-frequency intercept with the real impedance axis in a Nyquist plot gives the ohmic resistance. Often, however, also the low frequency intercept gives the resistance, due to other overlaying effects. Alternatively, the ohmic resistance can be measured using a current interruption technique in which a high-frequency symmetric square wave current is supplied to the outer electrodes. The voltage drop between the inner electrodes can be measured using an oscilloscope. The technique can preferably be used in parallel to the AC technique, since it provides information that facilitates the interpretation of the impedance data.

To some extent, conductivity measurements in a through-plane cell depend on the compressive forces on the membranes, and it is recommended to adjust the pressure to a fixed value by using a torque meter. The contact pressure should be enough to guarantee a good contact, but should also be as low as possible. With increasing temperature, dimensions of the membrane samples will change due to thermal expansion, which is expected to have opposite influences on the conductivity of the two types of cells. As little information is available for the membrane thermal expansion, this effect is generally ignored and the conductivity is calculated from the measured resistance using the initial room temperature dimensions. The atmospheric humidity should be carefully controlled and well specified in measurements of conductivity as well as other properties.

6.4.3 Temperature Dependence and Activation Energy

Conduction of protons is an activated process and the temperature dependence of the conductivity follows the Arrhenius equation as show in (6.17), where E_a is the activation energy for the proton conduction, R the gas constant, T is the absolute temperature, and A is the pre-exponential coefficient.

$$\sigma = A \exp\left(-\frac{E_a}{RT}\right) = \frac{\sigma_0}{T} \exp\left(-\frac{E_a}{RT}\right) \quad (6.17)$$

Physically the proton conductivity is influenced by the concentration of proton carriers and their mobility. In some cases, the temperature dependency may be more complex and cause deviation from the linear relationship obtained by plotting the natural logarithm of the conductivity (S cm^{-1}) against the inverse absolute temperature [1000 K^{-1}] in an Arrhenius plot. For example, at temperatures above, say 180–200 °C, the resistance of PA-doped membranes increases due to condensation of phosphoric acid to acid anhydrides and ultimately to polyphosphoric acid. From the slope of the linear fit, the activation energy for proton conduction can be obtained. For PA-doped PBI membranes with an ADL above 5, the E_a values are found to be between 20 and 30 kJ mol^{-1}, which is in a typical range for the Grotthuss hopping mechanism . A better linearity is observed by plotting $T\sigma$ versus T^{-1}.

6.5 Solubility and Gel Contents

6.5.1 Solubility

Polymers typically need more time to dissolve than low molecular weight compounds, and often show strong swelling before complete

dissolution. Therefore, polymer powders or particles should be added to the solvent to avoid aggregation, which often slows down dissolution when the solvent is added to polymer powder or pellets. Polymer solubility can also be strongly affected by the degree of crystallinity and the presence of additives or impurities, even water.

Good solvents for PBI are polar aprotic solvents such as *N*,*N*-dimethylacetamide (DMAc), *N*-methyl-2-pyrrolidone (NMP) or dimethylsulfoxide (DMSO), and strong protic acids like phosphoric acid, sulfuric acid (risking sulfonation reactions), or methylsulfonic acid. In order to dissolve PBI in organic solvents, great care must be taken to remove all phosphoric acid traces from the polymer, since it strongly hinders dissolution in DMAc.

For processing of PBI, it is often dissolved in DMAc. Especially at a high PBI content, e.g., >20 wt%, formation of agglomerates reduces the shelf life of the solution, as indicated by an increase in solution viscosity and resin precipitation. Therefore, a small amount of LiCl (i.e., 1.5 wt%) may be added as stabilizer [20, 21]. Thin films prepared from such solutions can be washed to remove LiCl by immersion in water at 85 °C for 1 h [22]. To speed up the PBI dissolution, increased temperatures are often necessary. In some cases also pressure reactors are used to increase the temperature up to over 260 °C [23]. At these conditions, the water content of the polymer must be reduced by drying at >70 °C in vacuo and the water content of DMAc should be lower than 0.03 %, to avoid hydrolysis of the solvent. It was also reported that the solubility is reduced by the presence of oxygen, and an inert atmosphere (nitrogen or argon) was recommended [23].

6.5.2 Filtration of PBI Solutions

To get defect-free membranes, organic solvent-based polymer solutions should be filtrated before casting. For large volumes, a glass filter or membrane filter can be used. For smaller volumes (<50 mL) the losses may be too high, and filtration through a syringe filter (0.45 µm) with a threaded connector is the preferred method. Due to the high viscosity of polymer solutions, a high pressure needs to be maintained over a long time. There are commercial products for emptying syringes, but a cheap sealant gun from the hardware store works well enough (Fig. 6.5). However, a sufficient gap between the polymer solution and the piston should be maintained as a pressure reservoir and to prevent leakage.

Fig. 6.5 Simple apparatus for filtration of small volumes of polymer solution, based on a sealant gun, a syringe, and a syringe filter with threaded connector

6.5.3 Gel Content

Solubility properties of new polymers are often reported qualitatively, e.g., in terms of insoluble, partially soluble, soluble or very soluble and thus this kind of test is based on personal experience.

A more quantitative measure is the gel content (GC) as defined by (6.18), where $W_{initial}$ and $W_{residual}$ are the initial and residual weight of a polymer membrane sample before and after immersion in a solvent for a certain period of time, respectively.

$$GC\ [\%] = 100 \cdot W_{residual}/W_{initial} \qquad (6.18)$$

A high gel content means that the membrane does not dissolve in the tested solvent. It is especially useful for the characterization of crosslinked membranes. The gel content correlates with the degree of crosslinking and the gel content can be used to compare the effectiveness of different crosslinking methods.

For both gel contents and qualitative solubility tests, membrane samples of similar thickness are immersed in the respective solvent, and kept at a fixed temperature for a fixed period of time, typically a few days. After the test, the membrane sample is dried and weighed to give $W_{residual}$. If the solution is stirred, care must be taken that the membrane is not hit by the stirrer to prevent mechanical degradation. For this purpose, the membrane samples can be protected by a sieve or wire mesh. In case the membrane disintegrates the solution can be filtrated and the dissolved portion can be determined by evaporation of the solvent.

6.6 Mechanical Properties

6.6.1 Tensile Stress and Strain

The most common mechanical testing method for membranes is tensile testing. In these tests membrane specimens with an initial length L_0, width w_0 and thickness d_0 are mounted between a fixed grip and a moveable grip. The force needed to stretch the material is plotted as a function of elongation to give a stress–strain curve.

When an axial force F is applied, the sample is stretched to the length L. The strain or elongation (ε) is defined as the gauge length of the specimen divided by its original length in percentage (100 %) or mm/mm according to (6.19).

$$\varepsilon[\mathrm{mm/mm}] = (L_0 - L)/L_0 \qquad (6.19)$$

Since the cross-sectional area of the sample during stretching can hardly be assessed, practically the initial dimensions are used in the calculation of the stress (engineering stress), as given by (6.20).

$$\sigma_E\ [\mathrm{MPa}] = F/(w_0 \times d_0) \qquad (6.20)$$

The tensile strength of a membrane is the maximum tensile stress that a sample can be subjected to before failure. Since the tensile strength is measured in units of force per unit area, it is basically a pressure and commonly expressed in pascals (Pa).

6.6.2 Tensile Testing

A standard procedure for testing thin films is given by ASTM D 882, which was developed for polymer films thinner than 1 mm. The widely used equipment for measuring mechanical properties is the universal materials strength testing machine. The standard sample geometry is that of 1 in. (2.53 cm) broad and 6 in. (15.24 cm) long rectangular stripes. However, most research groups use smaller sample sizes, e.g., 1 cm broad and 3 cm long, to reduce the amount of material. The crosshead speed is often chosen in the range of 5–10 mm min^{-1}. Some groups also chose slower initial speeds, e.g., 1 mm min^{-1} until 1 % elongation, to get more reliable data for the Young modulus, since mechanical properties depend on the strain rate.

A typical stress–strain curve for a polymer membrane is shown in Fig. 6.6, from which the ultimate tensile strength, tensile strength at break, Young modulus, elongation at break, proportional limit stress and proportional limit strain can be extracted. The area under the curve is proportional to the overall energy needed to break the material.

The Young's modulus or elastic modulus is given by the initial slope of the linear part of the curve. This is the part of the curve, in which the dislocation of the sample is practically

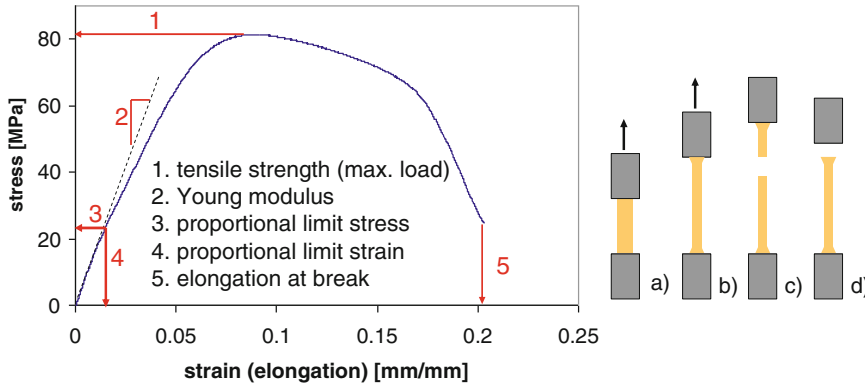

Fig. 6.6 Generic stress–strain curve of a polymer membrane; (**a**) membrane clamped into the testing machine at the beginning of testing, (**b**) during the test, (**c**) successful end of test, (**d**) failed test

reversible, i.e., the elastic deformation region. The units for stress and strain should be MPa and mm/mm, respectively. While all mechanical properties give valuable information, the Young modulus correlates with the resistance to be compressed or stretched and may thus be the most important parameter in this connection.

The yield strength is often used, defined as the stress at which material strain changes from elastic deformation to permanent deformation. At this point, the proportional limit stress and strain are defined after which the curve deviates from linearity to exhibit the plastic deformation. In some cases, for example for pristine PBI membranes under dry atmosphere, the tensile strength at yield is the maximum point of the curve. For acid-doped PBI membranes where a significant plasticizing effect is present, the stress values increase further after the yield point [1], reaching the ultimate tensile strength, the peak stress on a stress–strain curve. After a period of necking, the membrane eventually ruptures. The stress on the sample at the time of rupture is called the (engineering) tensile stress at break and the strain the elongation at break.

In addition to the phosphoric acid content, the water uptake or atmospheric humidity, as well as the temperature influence the mechanical properties of membranes. These effects are shown in Fig. 6.7 where *meta*-PBI membranes were tested at 21 and 150 °C under different water activities.

It is noteworthy that most tensile test machines do not provide humidity- and temperature-controlled atmospheres, and most literature data of tensile properties are obtained without specifications of the atmospheric humidities. Therefore, it is recommended to equilibrate the samples in ambient air before the test, and to record the ambient temperature and humidity, so that data can be reproduced and compared.

The standard deviation for tensile tests can be relatively high due to microscopic defects, and the number of tested specimens should be stated. Care must be taken so that the samples are not broken at the grips (Fig. 6.6d), which would lead to irreproducible results. This can be prevented by either the use of rubber-coated grips or, if rubber-coated grips are not available, by protecting the clamped part with tape. Cracks can grow from indentations at the edge of the sample and to prevent premature failure, it is recommended to cut the sample with a sharp blade.

6.6.3 Indentation, Compression, and Creep

In the fuel cell, the membrane is clamped between the electrodes, and is subjected to strong compressive forces. To evaluate the stability of PA-doped PBI membranes, imprint tests and

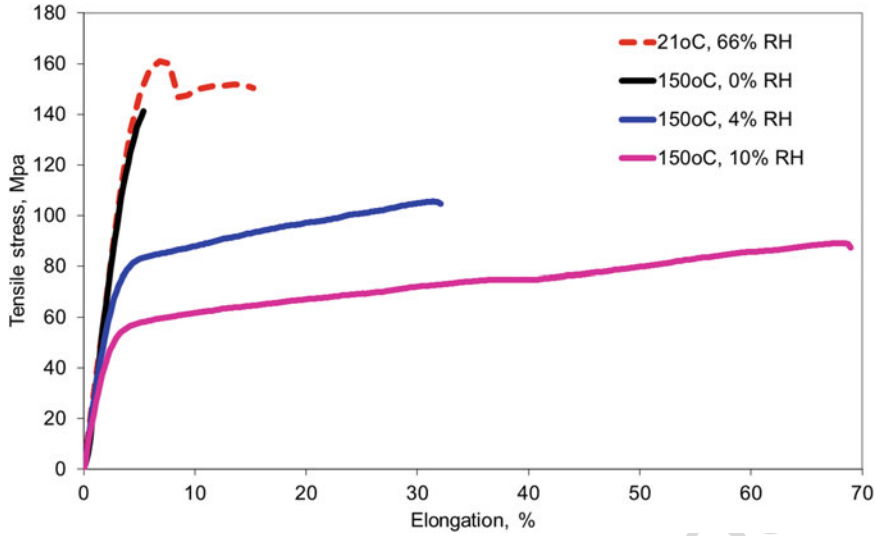

Fig. 6.7 Stress–strain curves of meta-PBI membranes ($M_w = 31{,}000$ g mol^{-1}) obtained at different temperatures and atmospheric humidities

compression creep tests were developed. In static imprint tests [24], a stamp is pressed on a PA-doped membrane at a given temperature (e.g., 200 °C) and under constant load. After the test time, the depth of the imprint is measured and reported as percentage of imprint depth. This test is mainly useful for rapidly comparing the properties of different membrane materials.

In compression creep tests, a flat disk-shaped membrane sample (i.e., 6.3 mm diameter and 0.9–1.2 mm thickness) is positioned between two sample holder plates of a dynamic mechanical analyzer (DMA) [25]. The creep compliance [Pa^{-1}] is obtained by dividing the strain with the applied stress (i.e., 0.1 MPa), and is usually displayed as a plot against the testing time. The creep rate is the slope of the resulting curve. Low compliance and creep rate are characteristics for a material with good creep resistance. Molleo et al. [25] found that the conditioning of the samples is vital for reproducible results, and recommend to store the samples sandwiched between two solid blocks at 180 °C (same as the test temperature) for about 24 h prior to the measurements, to get flat samples in which the PA is well distributed.

6.6.4 Dynamic Mechanical Analysis

Dynamic mechanical analysis (DMA) is also used for measuring the glass transition temperature (T_g) and the storage and loss modulus [26, 27]. The method allows also to measure the change of mechanical properties with the temperature, either in air, or in a liquid medium. This is not easily done in universal testing machines used for tensile strength tests. In general, a small membrane sample is clamped in the machine, and a very small force is repeatedly applied to the sample. If the force (e.g., expansion as in tensile strength tests) is below the proportional limit stress, each cycle should give a reproducible polymer response without degrading the mechanical properties. The measured response of the polymer to an applied stress is strain, the expansion of the sample. When a sinusoidal changing force is applied, the extension of the sample will follow with a small time shift, the phase angle δ. The maximum strain can be used to calculate the storage modulus E' (the elastic response of the system). From E' and δ, the loss modulus E'' can be calculated according to (6.21), which can be understood as the damping,

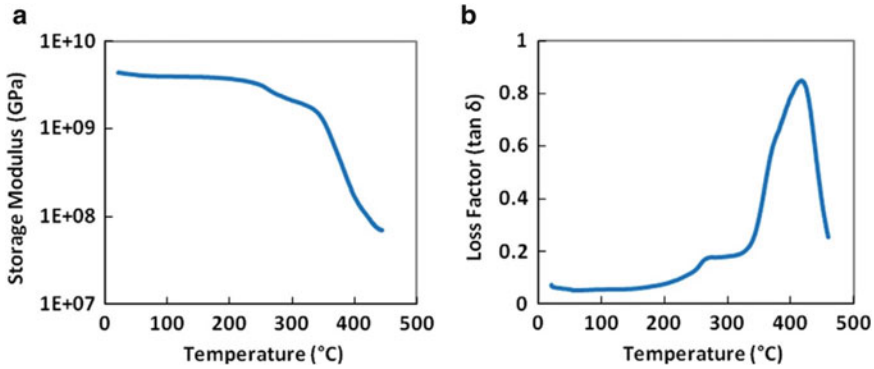

Fig. 6.8 Storage modulus and loss factor of polybenzimidazole as a function of temperature. Reproduced from [28] with permission of Elsevier

which occurs when some of the applied mechanical energy is lost, e.g., by change into internal motion (proportional to E'') or loss to the surroundings.

$$\tan\delta = E''/E' \tag{6.21}$$

When the storage modulus E' is plotted (logarithmically) against the temperature, many materials will show plateau areas (constant modulus) and areas where the modulus changes (see Fig. 6.8a). The latter areas are assigned to phase transitions, e.g., to the T_g. For reproducibility, it is necessary to state how the T_g is obtained from the curve, some workers use the onset of decreasing modulus, some use the point of the most negative slope. The T_g can also be obtained by a plot of tan δ against the temperature. This gives a peak, whose maximum can be used to describe the glass transition temperature (Fig. 6.8b). The smaller peak below 300 °C stems from the β relaxation, rotation and oscillation of side groups, while the T_g, the α relaxation, arises from movements of the polymer backbone.

6.7 Permeability, Methanol Crossover, and Electroosmotic Drag

Because of PBI's rigid structure and high degree of hydrogen bonding, PBI membranes have a close chain packing, leading to a density of 1.34 g cm^{-3} and very low gas permeability. When doped with acid, however, the membranes are swollen, resulting in a significant separation of the polymer backbones. This significantly increases the gas permeability and liquid crossover. Different techniques have been developed for the characterization.

6.7.1 Gas Permeabilities

The gas permeability of membranes can be measured by means of a two-chamber cell, as shown in Fig. 6.9. The two chambers have different pressures of up to 10 bar, and are separated by a membrane sample, which is supported by porous carbon or metallic mesh and sealed by, e.g., Viton® gaskets [29].

The net gas permeation is from the high pressure cell to the low pressure cell. For highly permeable membranes, it is possible to measure the gas flow volumetrically. This method can also be applied to measure the gas permeability of water-swollen membranes [30]. Alternatively, the variation of pressure with time can be monitored using pressure sensors [9]. This method is particularly suitable for dry membranes, because both cells are usually evacuated before the measurement. The gas diffuses through the membrane, driven by the pressure gradient. The amount of gas passed through the membrane can be calculated from (6.22), where n is the

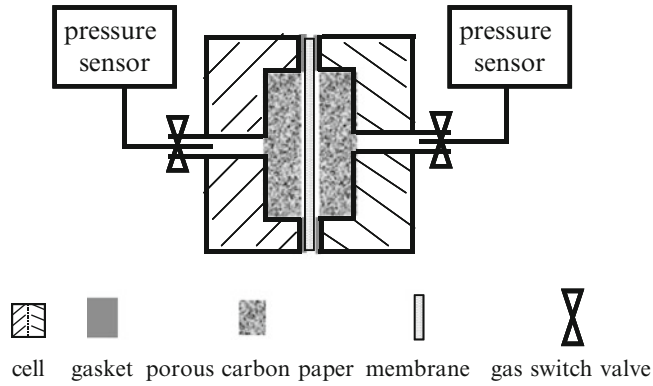

Fig. 6.9 The cell configuration for gas permeability measurement. Reproduced from [29] with permission of Elsevier

t.1 **Table 6.2** Gas permeability (10^{-17} mol cm cm^{-2} s^{-1} Pa^{-1}) [29]

t.2		H_2 permeability				O_2 permeability			
t.3		25 °C	80 °C	120 °C	180 °C	25 °C	80 °C	120 °C	180 °C
t.4	Nafion	4.1	15.7	–	–	2.8	3.1	–	–
t.5	PBI	–	1.6	3.0	4.3	–	0.05	0.06	0.1
t.6	PBI·6 H_3PO_4	–	120	250	380	–	30	70	90

mole number, Δp is the pressure difference, R is the gas constant, T is the absolute temperature, and V is the cell volume.

$$n = \frac{\Delta p \cdot V}{RT} \tag{6.22}$$

The gas permeability coefficient (P) can subsequently be calculated according to (6.23), where t is the time, L is the membrane thickness, A is the membrane area, and Δp is the pressure gradient across the membrane [31]. A common unit for presenting permeability data is the Barrer, 10^{-10} cm^3(STP) · cm · cm^{-2} · s^{-1} · cmHg^{-1}, STP being standard temperature (0 °C) and pressure (1 atm) [31].

$$P = \frac{n}{t} \cdot \frac{L}{A \cdot \Delta p} \tag{6.23}$$

For both undoped and PA-doped PBI, an increase of the gas permeability with temperature has been observed (Table 6.2) [29]. While pure PBI (as many other hydrocarbon-based polymers) [32] shows about ten times lower hydrogen permeability than Nafion®, the hydrogen permeability of PA-doped PBI is roughly one order of magnitude higher than that of Nafion®. Furthermore, the hydrogen permeability is usually higher than that of oxygen [29].

In addition, the permeability (P) is the product of the gas diffusion coefficient (D) and the solubility (C) of the gas in the polymer. As the gas solubility in a polymer is in a low range, Henry's law can always be assumed. The Henry's constant, also called the solubility coefficient ($k = Cp^{-1}$), is a constant over the pressure range. Here C is the solubility of the gas in the polymer and p is the pressure. From the measured permeability and Henry's constant, one can calculate the diffusion coefficient of the relevant gases.

6.7.2 Electrochemical Stripping Method for Hydrogen Permeability Measurements

When the cathode of an H_2-air fuel cell is switched from air to nitrogen or argon, the oxygen in the cathode chamber will be depleted and the open circuit voltage (OCV) decreases until a steady state is reached. At this point, the potential

is not zero because the concentration gradient drives hydrogen through the membrane to the cathode by diffusion. A concentration cell is eventually established with pure hydrogen on one side and trace hydrogen in nitrogen or argon on the other. An electromotive force is developed following the Nernst equation (6.24).

$$\mathrm{EMF} = \frac{RT}{nF} \cdot \ln \frac{P^1_{\mathrm{H_2}}}{P^2_{\mathrm{H_2}}} \tag{6.24}$$

Considering $P^1_{\mathrm{H_2}} = 1$ atm and $P^2_{\mathrm{H_2}} = 0.001$ atm, for example, the above equation gives an EMF of 89 mV at room temperature. In practice the hydrogen electrode is connected to the counter and reference terminals of a potentiostat while the nitrogen electrode is connected to the working electrode (and sensor as well). In a typical linear voltage sweep (LSV) experiment the potential is now increased from, e.g., 0.1 to 0.6 V (see, e.g., Fig. 17.6 in Chap. 17). More positive potentials above 600 mV versus hydrogen reference should be avoided to prevent oxidative side reactions like platinum oxidation. Below the potential of the established concentration cell, a negative current will be measured, and the cell works as a concentration cell. However, if the external potential is high enough to oxidize the trace hydrogen in the nitrogen stream, an oxidation current will be measured. This positive current depends on the hydrogen permeation rate and therefore is a function of the hydrogen partial pressure, the temperature and humidity, and ideally gives a straight line parallel to the *x*-axis. A positively sloped curve indicates the existence of some shorting (ohmic resistance), as discussed in Chap. 17. In practice, it happens from time to time that only negative currents are measured throughout the whole tested potential range. In this case, the cell or tubings are not perfectly sealed, and the cell still operates as a hydrogen/air fuel cell.

In most cases, a linear fit of the linear, positive part of the LSV curve to 0 V reflects well the hydrogen crossover current. However, the oxidation current under the voltage sweeping contains also contributions of the double layer charging current, especially at high sweep rates. In principle a background current under the N_2–N_2 mode should be measured and used for correction of the hydrogen oxidation current. Alternatively, assuming that other contributions are small in comparison to the hydrogen crossover, a constant potential of 0.4 V can be applied and the oxidation current of the permeated hydrogen is recorded as a function of time until a steady-state value is reached [33]. For most purposes, the electrochemically measured hydrogen stripping current density can be converted into the hydrogen permeability in mol H_2 cm^{-1} bar^{-1} s^{-1} according to (6.25), where i is the hydrogen crossover current density, L is the membrane thickness, Δp is the pressure gradient of hydrogen across the membrane, n is the number of electrons involved in the hydrogen oxidation, and F is the Faraday constant.

$$P_{\mathrm{H_2}} = \frac{i}{nF} \cdot \frac{L}{\Delta p} \tag{6.25}$$

As an example, Cleemann et al. [33] obtained a value around 1.9×10^{-10} mol cm^{-1} s^{-1} bar^{-1} at room temperature for a 40 µm-thick PBI membrane doped with 8 mol PA per repeat unit.

6.7.3 Methanol Crossover

Although PA-doped PBI is mainly used for fuel cells fed with hydrogen or hydrogen rich reformate, it has also been evaluated as electrolyte material in direct methanol fuel cells. Several different procedures for determining the methanol crossover have been proposed.

Similar to the hydrogen crossover, the methanol permeability of membranes can be investigated in a fuel cell setup. The fuel cell cathode is connected to a potentiostat as the working electrode and flushed with nitrogen. The fuel cell anode is connected to the potentiostat as the counter electrode. The potential of the cathode is potentiostatically held at a high potential, e.g., 0.9 V or 1.1 V versus a hydrogen reference electrode [34, 35]. Methanol

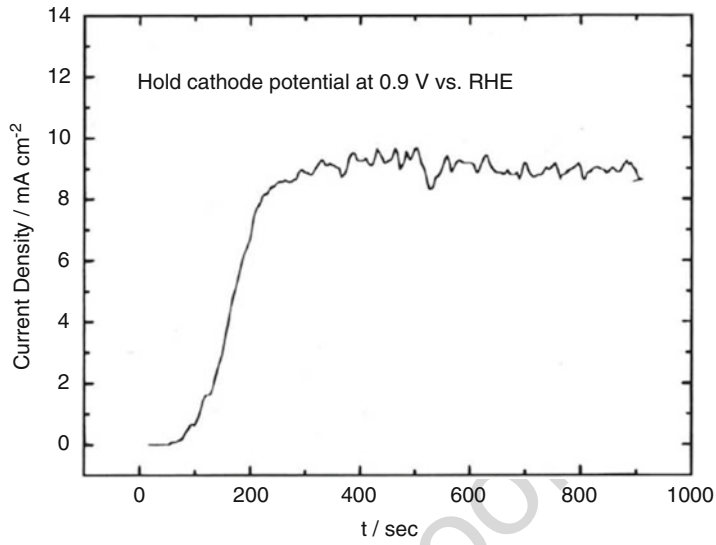

Fig. 6.10 Methanol oxidation current measured at the cathode versus time during the introduction of a water/methanol mixture to the anode. Cathode potential: 0.9 V versus RHE; Membrane: PBI doped with ADL = 5 and thickness of 0.008 cm; temperature: 150 °C. Reproduced from [34] with permission of The Electrochemical Society

is then introduced into the anode chamber while the current at the cathode is monitored. This high potential is essential to ensure a complete oxidation of the methanol that has permeated through the membrane. The obtained steady-state current is assumed to be the direct measure of the methanol crossover rate. As shown in Fig. 6.10 a time-independent current of ca. 9 mA was obtained after 250 s.

In another method, the CO_2 content of the cathode gas stream is monitored. By keeping a methanol or a water/methanol mixture flow through the anode chamber, methanol steadily permeates through the membrane to the cathode. By holding the cathode potential at OCV to avoid electroosmotic drag of methanol, it is assumed, again, that all permeated methanol is oxidized into CO_2 which is carried out of the cell by the cathode air stream. A mass spectrometer [34] or an infrared sensor [36] have been used to measure the CO_2 content. The methanol crossover rate can be determined by using (6.26), where i_{MeOH} is the methanol crossover rate expressed as a current density, $\dot{V}_{air}$ is the air flow rate under standard conditions ($p_0 = 1$ atm, $T_0 = 273$ K), $X_{O_2} = 0.209$ is the concentration of oxygen in air, λ is the oxygen flow stoichiometry, X_{CO_2} is the concentration of CO_2 in the cathode exhaust

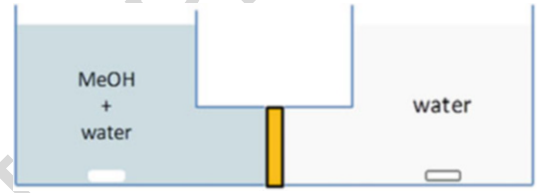

Fig. 6.11 Diffusion cell for measurement of methanol permeability with a membrane clamped between the two compartments and magnetic stir bars

stream, A is the active area of the cell, R the gas constant, and F is the Faraday constant [36].

$$i_{MeOH} = \dot{V}_{air}\left(1 - \frac{X_{O_2}}{\lambda}\right)X_{CO_2}\frac{p_0}{RT_0}\frac{6F}{A} \quad (6.26)$$

Methanol permeation can also be measured in a diffusion cell. One side of the membrane is in contact with a water-based methanol solution, the other with pure water (Fig. 6.11). The concentration gradient results in diffusion of methanol to the water reservoir, without any interference by electroosmotic drag. The increasing methanol concentration in the water-filled cell is monitored by gas chromatography [37], changes in the refractive index [38] or density [39]. While this method is very useful for sulfonated membranes like Nafion®, it cannot

be used for PA-doped membranes, because PA would leach out. A detailed description of the measurement and the underlying physical principals can be found in [37].

6.7.4 Electroosmotic Drag of Water

In the fuel cell, protons move through the electrolyte from the anode to the cathode. While over 95 % of the conduction in PA-doped PBI membranes is based on a Grotthus-type conduction mechanism [40], also the vehicular mechanism is observed. Since protons do not exist as naked protons in condensed matter, but rather as solvated protons (e.g., H_3O^+, $H_5O_2^+$ or $H_4PO_4^+$) in PA-doped PBI, these protons move together with their solvation shell, resulting in flow of the proton solvent from the anode to the cathode, the so-called electroosmotic drag. In typical PA-doped PBI, the electroosmotic drag of water molecules is close to 0 [41] but is expected to increase when water-based methanol solutions are used as fuel. For Nafion® membranes, the electroosmotic drag coefficient (water molecules per proton) decreases with the current and depends on the membrane humidity. Unfortunately the direction of this dependence is not clear [42, 43].

The electroosmotic drag (EOD) of water molecules in a running fuel cell can be obtained from the balance [36]:

$$\begin{aligned}\text{cathode}_{\text{out}} = {} & \text{cathode}_{\text{in}} + \text{product water} \\ & + \text{water from side reactions} \\ & + \text{EOD} + \text{concentration driven} \\ & \text{water permeation.}\end{aligned}$$

The water which leaves the cell ($\text{cathode}_{\text{out}}$) can be obtained gravimetrically by condensing water from the gas stream in a cooling trap. $\text{Cathode}_{\text{in}}$ can be set to zero (anhydrous gas stream) or be measured in a dummy cell [36]. The produced water can be calculated from the current. Concentration driven diffusion of water can be observed from the anode to the cathode, if humidified anode gas streams are used, but may also be reverted, when the cathode humidity increases at high currents due to high water production (water-back diffusion). Water can also be formed in side reactions, e.g., when methanol crosses over to the cathode and is directly oxidized to water and CO_2. This term can be estimated through electrochemically obtained methanol permeation measurements (linear sweep voltammetry) [36].

A simple approach to measure the EOD of a membrane is to run a fuel cell in the hydrogen pumping mode, in which the anode stream is humidified hydrogen or methanol and the cathode stream is dry or only partially humidified hydrogen. In this mode, the fuel is oxidized at the anode, and the resulting protons migrate to the cathode, where they are reduced to hydrogen. This eliminates the contributions of water production, water producing side reactions, and water-back diffusion. All water found in the cathode exhaust gas stream either permeated to the cathode driven by the set humidity gradient (water flux at OCV, a constant value independent of the current), or was transported by EOD (current >0 A) [43]. Instead of condensing water from the gas streams in a fuel cell setup, it is also possible to use closed volume cells separated by a membrane electrode assembly, and to measure the pressure changes of the anode and cathode cell in relation to the electric current [41].

For PA-doped PBI, the contribution of the mobile acid anion species to the conductivity is of great concern from both theoretical and engineering point of view.

6.8 Thermal and Oxidative Stability

6.8.1 Thermal Stability

The thermal stability of polymers can be tested by thermogravimetric analysis (TGA). In this method, a sample of a few milligrams is deposited in a scale pan mounted on a furnace. TGA measurements can be done in isothermal mode by maintaining a certain temperature for a fixed period of time or in temperature cycling mode. Most often the data are obtained with a constant

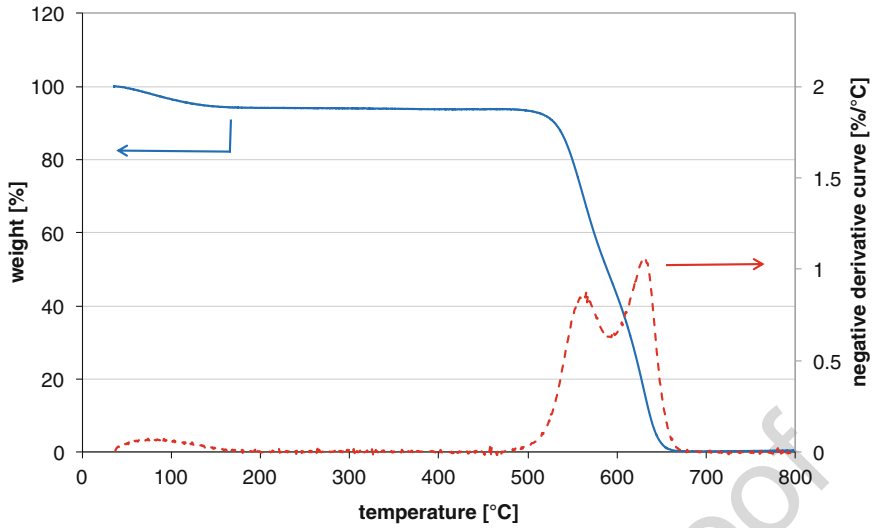

Fig. 6.12 TGA and derivative curve of a membrane made from meta-PBI (Dapozol®) recorded in air atmosphere and with a heating rate of 10 °C min^{-1}

heating rate. During the measurement, a heated gas stream passes the pan, and the temperature of the gas stream is increased with a constant heating rate. Plotting the weight or the normalized weight against the temperature gives the TGA curve. The first weight loss often stems from water that is not completely removed by drying the sample or is reabsorbed during handling of the dried membrane in ambient atmosphere (Fig. 6.12). To remove traces of high boiling-point solvents like DMAc or NMP, it can be necessary to immerse membranes in water before preparing TGA samples. The dotted line in Fig. 6.12 is the derivative curve, i.e., the slope plotted against the temperature. This representation gives basically the same information, but in some cases, when degradation processes overlap, peak fitting can give access to information hidden in the TGA curve.

While most organic materials are completely oxidized to volatile species in air, inert atmosphere (typically nitrogen or argon) leads to formation of soot, and a significant residual weight. It should be remarked that the TGA curve does not represent a thermodynamic equilibrium, but kinetically controlled degradation processes. Therefore, TGA data is not complete without mentioning the atmosphere and heating rate. In fact, while *meta*-PBI appears to be stable at temperatures up to 500 °C as shown in Fig. 6.12, a more precise conclusion is that the material is stable at 500 °C within the time scale of the measurement. The long-term thermal stability of a material cannot be deducted from a single TGA curve. For quantitative comparison of materials, a commonly used description of TGA data is to give the temperature at which 3 or 5 % weight loss (ignoring water and solvent evaporation) is observed.

Since TGA curves represent kinetic processes, it is possible to estimate the activation energy of the degradation reaction from TGA data, as shown by Flynn and Wall [44]. For this purpose, it is necessary to measure the TGA curves of a material at different heating rates. From these curves, the temperature at, e.g., 5 % weight loss is extracted and plotted in an Arrhenius plot, i.e., the natural logarithm of the heating rate β against $1000/T(\mathrm{K})$. This representation gives a linear trend with a negative slope, which is proportional to the activation energy E_a of the investigated degradation step. The activation energy can be obtained according to (6.27), where b is a constant and needs to be obtained by iteration.

However, for values of E_a/RT between 29 and 46, b is 0.457 ± 1 % [44–46].

$$E_a = -[d(\log\beta)/d(1/T)] \times (R/b) \qquad (6.27)$$

Limitations with this method are the necessity of well-resolved degradation steps without overlapping reactions, first-order kinetics and no dependence of the degradation mechanism on the conversion level. With the help of the estimated activation energy, it is also possible to predict the lifetime of a material at a given temperature, according to Toop [45, 47].

6.8.2 Oxidative Stability by Fenton Test

The gas crossover, as discussed above, leads not only to losses in the efficiency, but is also expected to form active oxygen species such as peroxides, hydroperoxy radicals, and hydroxy radicals. For Nafion® based systems it was shown that reactive oxygen species form especially when oxygen crosses over to the anode [48]. These aggressive species attack organic polymers and lead to chemical degradation. In comparison to Nafion®, PA-doped PBI membranes have a relatively large gas permeability, and thus a large amount of reactive oxygen species may be present in the electrodes and be dragged or diffused to the membrane, where the polymer will be attacked.

To compare different polymers with respect to their chemical stability, the Fenton test is widely applied in fuel cell membrane research. In these tests, membrane samples are immersed in hydrogen peroxide solution containing a small amount of Fe^{2+}, e.g., iron(II)sulfate. In the presence of the metal ion, the decomposition of hydrogen peroxide is accelerated. The ongoing reactions are very complex, and several reactive intermediates are formed. Just as an example and demonstrating the catalytic nature, the following partial reactions of the so-called Haber–Weiss mechanism are highlighted, as shown in (6.28)–(6.31) [49, 50].

$$Fe^{2+} + H_2O_2 \rightarrow HO^{\bullet} + OH^- + Fe^{3+} \qquad (6.28)$$

$$Fe^{2+} + HO^{\bullet} \rightarrow Fe^{3+} + OH^- \qquad (6.29)$$

$$H_2O_2 + HO^{\bullet} \rightarrow HOO^{\bullet} + H_2O \qquad (6.30)$$

$$Fe^{3+} + H_2O_2 \rightarrow Fe^{2+} + HOO^{\bullet} + H^+ \qquad (6.31)$$

Obvious shortcomings of Fenton tests are their strong dependence on not standardized test protocols and the often qualitative nature of the monitored parameter, e.g., time until the membrane breaks or when floccules start to precipitate (see Table 6.3). Even within one paper, several test conditions may be used in parallel. Furthermore, due to the thermal instability of peroxide solutions, the solutions must be refreshed regularly. Sometimes, samples are immediately re-immersed, in other cases, samples are washed

Table 6.3 Selected literature examples for Fenton tests

$[H_2O_2]$	$[Fe^{2+}]$	Conditions	Characterizations	Reference
(a) 30 %	(a) 20 ppm	(a) RT; 0, 8, 16, 24 h	IR, NMR, weight loss and time until floccules could be observed in the solution	[51]
(b) 3 %	(b) 2 ppm	(b) 80 °C; 24 h		
3 wt%	20 ppm	(a) 40 °C; 24 h	Weight loss	[52]
		(b) 160 °C; 24 h		
a) 3 %	a) 4 ppm	Fresh solution:	Weight loss, visual observation, conductivity after PA doping	[53]
b) 30 %	b) 20 ppm	(a) every 24 h, 20 cycles at 70 °C		
		(b) every 18 h, 3 cycles at 85 °C		
3 %	4 ppm	68 °C; fresh solution every 20–24 h; 200 h	Weight loss	[1]

with water, dried, and then weighed before re-immersion. Comparison of data from different publications is practically impossible.

In brief, the Fenton test for pristine PBI membranes is informative as an aging tool for qualitative comparison of the chemical stability of different materials. However, the test is apparently an overdoing method. The materials that withstand the test are surely durable in the real fuel cells, but those that cannot survive the test might still be sufficiently durable in fuel cells.

A more critical issue concerns the effect of the phosphoric acid, which as a dopant is always present in the membrane. Most of Fenton studies in literature have been performed in the absence of phosphoric acid. As recently pointed out by Liao et al. [54], the presence of phosphoric acid makes the situation more complicated since it forms complexes with metal ions and thus inhibits the H_2O_2 decomposition. Additionally, the lowered pH of the solution further prevents the decomposition of H_2O_2. Phosphoric acid present in the Fenton solution will also interact with the N–H groups of PBI, swelling the polymer and thus facilitating the access of the peroxide radicals to the macromolecular chains.

6.9 Humidity Definition and Control

6.9.1 Saturated Water Vapor Pressure, Relative Humidity, and Dew Point

Virtually all physicochemical properties of a polybenzimidazole membrane are strongly dependent on the water content, and it is thus important to investigate the membrane characteristics under humid conditions at elevated temperatures [55]. The membrane is highly hydrophilic and the equilibrium water content within the membrane is developed rather fast. At temperatures below or around 100 °C there is a risk that water condenses on the membrane at high water partial pressures, i.e., when the temperature falls below the dew point. Condensation of water on the membrane gives a poorly defined two-phase system and leaches out phosphoric acid. As shown in Fig. 6.13, the saturated vapor pressure of water increases dramatically at temperatures above 100 °C, which reduces the risk for condensation.

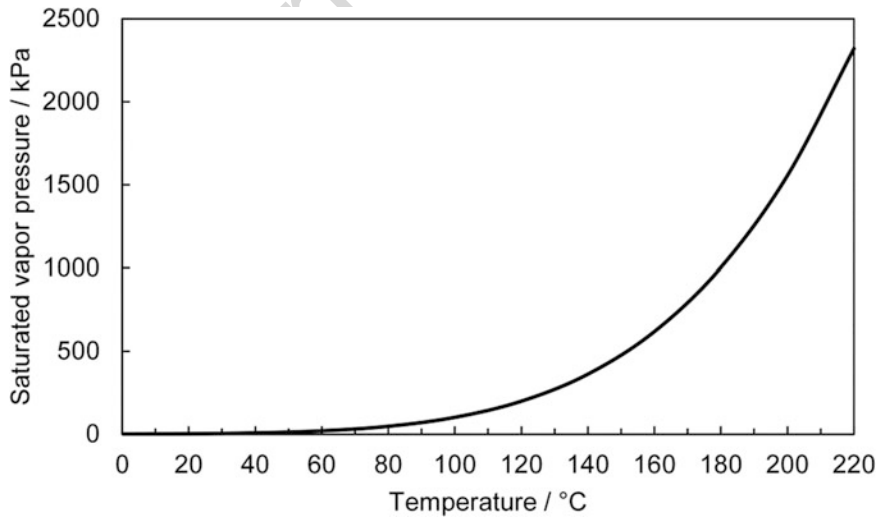

Fig. 6.13 Saturated vapor pressure of water as a function of temperature [56]

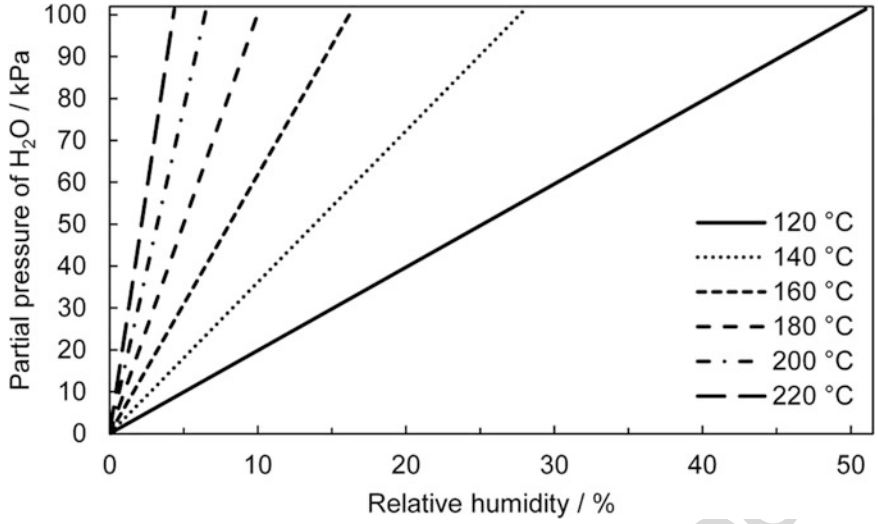

Fig. 6.14 The corresponding partial pressures of water at different relative humidity in the temperature range relevant for high-temperature polymer electrolyte membrane fuel cells

The relative humidity (RH), which is often used to specify the water content in the atmosphere, is defined as the ratio (in percent) of the partial pressure of water vapor (P_{H_2O}) and the saturated vapor pressure of water at that particular temperature (P_{sat}) according to (6.32).

$$RH = P_{H_2O}/P_{sat} \quad (6.32)$$

At temperatures below 100 °C the relative humidity is a convenient measure to use. At temperatures above the dew point of water the use of RH can, however, be rather confusing. The relative humidity at different partial pressures of water at temperatures ranging from 120 to 220 °C is given in Fig. 6.14. At atmospheric absolute pressure, the partial pressure of water in kPa roughly equals the water content in mole or volume percent. It can be seen that the relative humidity at a particular partial pressure of water decreases dramatically with increasing temperature. For example, at 120 and 220 °C the pure steam atmosphere (P_{H_2O} = 101 kPa) corresponds to a relative humidity of 51 % and 4.4 %, respectively.

6.9.2 Control of Water Content

One convenient way to control the water content of a gas, particularly in the lower temperature range, is to bubble it through a water bath at a fixed temperature (sparging or dew point method). Assuming that the gas phase above the surface in the water bath is saturated with water vapor, the partial pressure of water in the gas stream can be calculated [57]. Generally it is of great importance that the temperature of all the tubing is carefully controlled so that condensation of water is avoided, otherwise water condenses at the point where the temperature is lower than the dew point.

Practically the partial pressure of water at temperatures above 100 °C can be controlled by pumping water into an evaporator and converge the steam with a secondary carrier gas [55]. The partial pressure of water in the obtained gas mixture can be adjusted by controlling the pumping rate of liquid water and the flow rate of the carrier gas. Due to the large volume expansion of water the pumping rate has to be delicately controlled at very low values and free from pulses.

In closed systems the partial pressure of water can be controlled using aqueous solutions of LiCl with different concentrations, which have well-defined liquid–vapor equilibriums [58, 59].

Acknowledgements The authors acknowledge funding by the Danish Agency for Science, Technology, and Innovation in the frame of the 4M project, KIST's K-GRL project and the Korea-Denmark green technology cooperative research program.

References

1. Yang JS, Cleemann LN, Steenberg T et al (2014) High molecular weight polybenzimidazole membranes for high temperature PEMFC. Fuel Cells 14:7–15
2. Yuan Y, Johnson F, Cabasso I (2009) Polybenzimidazole (PBI) molecular weight and Mark-Houwink equation. J Appl Polym Sci 112:3436–3441
3. Buckley A, Stuetz D, Serad GA (1987) Polybenzimidazoles. In: Kroschwitz JI (ed) Encyclopedia of polymer science and engineering. Wiley, New York, pp 572–601
4. Savinell RF, Wainright JS, Litt M (1998) High temperature polymer electrolyte fuel cells. In: Gottesfeld S, Fuller TF (eds) Electrochemical Society Series. 98(27):81–90
5. Kojima T, Yokota R, Kochi M et al (1980) Dilute solution properties of a polybenzimidazole. J Polym Sci B 18:1673–1683
6. Liao JH, Li QF, Rudbeck HC et al (2011) Oxidative degradation of polybenzimidazole membranes as electrolytes for high temperature proton exchange membrane fuel cells. Fuel Cells 11:745–755
7. Choe EW, Conciatori AB (1985) Aminoaryl ester reactant, two-stage melt polymerization. US Patent 4,535,144
8. Gulledge AL, Chen X, Benicewicz BC (2014) Investigation of sequence isomer effects in AB-polybenzimidazole polymers. J Polym Sci A Polym Chem 52:619–628
9. Han JY, Lee JY, Kim HY et al (2014) Synthesis and characterization of fluorene-based polybenzimidazole copolymer for gas separation. J Appl Polym Sci 131:40521
10. Ng F, Bae B, Miyatake K et al (2011) Polybenzimidazole block sulfonated poly(arylene ether sulfone) ionomers. Chem Commun 47:8895–8897
11. Dominguez PH, Grygiel K, Weber J (2014) Nanostructured poly(benzimidazole) membranes by N-alkylation. eXPRESS Polym Lett 8:30–38
12. Huang W, Qing SB, Yang JT et al (2008) Preparation and characterization of soluble sulfonated polybenzimidazole for proton exchange membrane materials. Chinese J Polym Sci 26:121–129
13. Robinson RA (2005) The water activities of lithium chloride solutions up to high concentrations at 25°. Trans Faraday Soc 41:756-758
14. Li Q, He R, Berg RW et al (2004) Water uptake and acid doping of polybenzimidazoles as electrolyte membranes for fuel cells. Solid State Ionics 168:177–185
15. Majerus A, Conti F, Korte C et al (2012) Thermogravimetric and spectroscopic investigation of the interaction between polybenzimidazole and phosphoric acid. Abstract 1510. Paper presented at Honolulu PRiME 2012, Honolulu, 7–9 October 2012
16. Mader JA, Benicewicz BC (2011) Synthesis and properties of segmented block copolymers of functionalised polybenzimidazoles for high-temperature PEM fuel cells. Fuel Cells 11:222–237
17. Lee HJ, Lee DH, Henkensmeier D et al (2012) Synthesis and characterization of H_3PO_4 doped poly (benzimidazole-co-benzoxazole) membranes for high temperature polymer electrolyte fuel cells. Bull Korean Chem Soc 33:3279–3284
18. Li X, Chen X, Benicewicz BC (2013) Synthesis and properties of phenylindane-containing polybenzimidazole (PBI) for high-temperature polymer electrolyte membrane fuel cells (PEMFCs). J Power Sources 243:796–804
19. Hasiotis C, Li Q, Deimede V et al (2001) Development and characterization of acid-doped polybenzimidazole/sulfonated polysulfone blend polymer electrolytes for fuel cells. J Electrochem Soc 148: A513–A519
20. Hanley TR, Helminiak TE, Benner CL (1978) Expansion of aromatic heterocyclic polymers in salt solution. J Appl Polym Sci 22:2965–2978
21. Li X, Qian G, Chen X, Benicewicz BC (2013) Synthesis and characterization of a new fluorine-containing polybenzimidazole (PBI) for proton-conducting membranes in fuel cells. Fuel Cells 13:832–842
22. Leaflet "Polybenzimidazole (PBI) S26 Solution", PBI performance products, Inc. http://www.pbiproducts.com/images/uploads/main/Polymers/Solutions_Brochure.pdf
23. Murata M, Nakamura T (1999) Polybenzimidazole compounds in solution and a process for the preparation thereof. US Patent 5,902,876
24. Belack J, Kundler I, Schmidt TJ (2008) Celtec-MEAs: life time, degradation modes and mitigation strategies. Paper presented at Progress MEA 2008, La Grande Motte, 21–24 September 2008
25. Molleo MA, Chen X, Ploehn HJ et al (2014) High polymer content 3,5-pyridine-polybenzimidazole copolymer membranes with improved compressive properties. Fuel Cells 14:16–25
26. Frequently asked questions: dynamic mechanical analysis (DMA), a beginner's guide, booklet from Perkin Elmer. http://www.perkinelmer.com/CMSResources/Images/44-74546GDE_IntroductionToDMA.pdf

27. Dynamic mechanical analysis basics: Part 1: How DMA works. Technical note, Perkin Elmer. http://www.perkinelmer.com/CMSResources/Images/44-74304app_thermaldynmechanalybasicspart1.pdf
28. Iqbal HMS, Bhowmik S, Benedictus R (2014) Process optimization of solvent based polybenzimidazole adhesive for aerospace applications. Int J Adhes Adhes 48:188–193
29. He R, Li Q, Bach A et al (2006) Physicochemical properties of phosphoric acid doped polybenzimidazole membranes for fuel cells. J Membr Sci 277:38–45
30. Sakai T, Takenako H, Wakabayashi N et al (1985) Gas permeation properties of solid polymer electrolyte (SPE) membranes. J Electrochem Soc 132:1328–1332
31. Baker RW (2004) Membrane technology and applications, 2nd edn. Wiley, Chichester, p 304
32. Kim BG, Henkensmeier D, Kim HJ et al (2014) Sulfonation of PIM-1—towards highly oxygen permeable binders for fuel cell application. Macromol Res 22:92–98
33. Cleemann LN, Buazar F, Li Q et al (2013) Catalyst degradation in high temperature proton exchange membrane fuel cells based on acid doped polybenzimidazole membranes. Fuel Cells 13:822–831
34. Wang JT, Wasmus S, Savinell RF (1996) Real-time mass spectrometric study of the methanol crossover in a direct methanol fuel cell. J Electrochem Soc 143:1233–1238
35. Mamlouk M, Scott K, Hidayati N (2011) High temperature direct methanol fuel cell based on phosphoric acid PBI membrane. J Fuel Cell Sci Technol 8:061009
36. Gubler L, Kramer D, Belack J et al (2007) Celtec-V. A polybenzimidazole-based membrane for the direct methanol fuel cell. J Electrochem Soc 154: B981–B987
37. Tricoli V (1998) Proton and methanol transport in poly(perfluorosulfonate) membranes containing Cs^+ and H^+ cations. J Electrochem Soc 145:3798–3801
38. Woo Y, Oh SY, Kang YS et al (2003) Synthesis and characterization of sulfonated polyimide membranes for direct methanol fuel cell. J Membr Sci 220:31–45
39. Yang CC, Lee YJ, Yang JM (2009) Direct methanol fuel cell (DMFC) based on PVA/MMT composite polymer membranes. J Power Sources 188:30–37
40. Savinell RF (2012) Recent research of the PBI/PA system as a proton conductor in electrochemical systems. Presentation at Carisma 2012, Copenhagen, Denmark. http://www.hotmea.kemi.dtu.dk/~/media/Centre/ENRGK_HotMEA/carisma2012/presentations_posters/savinell_carisma_2012.ashx
41. Weng D, Wainright JS, Landau U et al (1996) Electroosmotic drag coefficient of water and methanol in polymer electrolytes at elevated temperatures. J Electrochem Soc 143:1260–1263
42. Luo Z, Chang Z, Zhang Y et al (2010) Electroosmotic drag coefficient and proton conductivity in Nafion membrane for PEMFC. Int J Hydrogen Energy 35:3120–3124
43. Peng Z, Morin A, Huguet P et al (2011) In-situ measurement of electroosmotic drag coefficient in Nafion membrane for the PEMFC. J Phys Chem B 115:12835–12844
44. Flynn JH, Wall LA (1966) A quick, direct method for the determination of activation energy from thermogravimetric data. Polym Lett 4:323–328
45. TA Instruments Application Brief TA-125. http://www.tainstruments.co.jp/application/pdf/Thermal_Library/Applications_Briefs/TA125.PDF
46. Yang HE, Chen LJ, He F et al (2012) NM Cable insulation service life time prediction using materials degradation kinetics. Proceedings of the 61st international wire & cable symposium (IWCS), pp 791–798. http://iwcs.omnibooksonline.com/data/papers/2012/16-5.pdf
47. Toop DJ (1971) Theory of life testing and use of thermogravimetric analysis to predict the thermal life of wire enamels. IEEE Trans Electr Insul EI-6:2–14
48. Inaba M, Kinumoto T, Kiriake M et al (2006) Gas crossover and membrane degradation in polymer electrolyte fuel cells. Electrochim Acta 51:5746–5753
49. Gubler L, Koppenol WH (2012) Kinetic simulation of the chemical stabilization mechanism in fuel cell membranes using cerium and manganese redox couples. J Electrochem Soc 159:B211–B218
50. Kinumoto T, Inaba M, Nakayama Y et al (2006) Durability of perfluorinated ionomer membrane against hydrogen peroxide. J Power Sources 158:1222–1228
51. Chang Z, Pu H, Wan D et al (2010) Effects of adjacent groups of benzimidazole on antioxidation of polybenzimidazoles. Polym Degrad Stab 95:2648–2653
52. Qian G, Benicewicz BC (2009) Synthesis and characterization of high molecular weight hexafluoroisopropylidene-containing polybenzimidazole for high-temperature polymer electrolyte membrane fuel cells. J Polym Sci A Polym Chem 47:4064–4073
53. Han M, Zhang G, Liu Z, Wang S et al (2011) Cross-linked polybenzimidazole with enhanced stability for high temperature proton exchange membrane fuel cells. J Mater Chem 21:2187–2193
54. Liao JH, Yang JS, Li QF et al (2013) Oxidative degradation of acid doped polybenzimidazole membranes and fuel cell durability in the presence of ferrous ions. J Power Sources 238:516–522
55. He RH, Li Q, Xiao G et al (2003) Proton conductivity of phosphoric acid doped polybenzimidazole and its composites with inorganic proton conductors. J Membr Sci 226:169–184
56. Wagner W, Pruss A (1993) International equations for the saturation properties of ordinary water substance - revised according to the international temperature scale of 1990. J Phys Chem Ref Data 22:783–787

57. Costamagna P, Srinivasan S (2001) Quantum jumps in the PEMFC science and technology from the 1960s to the year 2000: Part II. Engineering, technology development and application aspects. J Power Sources 102:253–269
58. Gibbard HF, Scatchar G (1973) Liquid-vapor equilibrium of aqueous lithium-chloride, from 25° to 100°C and from 1.0 to 18.5 molal, and related properties. J Chem Eng Data 18:293–298
59. Schechter A, Savinell RF, Wainright JS et al (2009) ^{1}H and ^{31}P NMR study of phosphoric acid-doped polybenzimidazole under controlled water activity. J Electrochem Soc 156:B283–B290